Journal of Magnetics 16(2), 150-156 (2011) DOI: 10.4283/JMAG.2011.16.2.150

A New Vibration Energy Harvester Using Magnetoelectric Transducer

Jin Yang*, Yumei Wen, Ping Li, Xianzhi Dai, and Ming Li

Key Laboratory for Optoelectronic Technology & Systems of Ministry of Education, College of Optoelectronic Engineering, Chongqing University, Chongqing City 400044, PR China

(Received 25 February 2011, Received in final form 10 April 2011, Accepted 14 April 2011)

Magnetoelectric (ME) transducers were originally intended for magnetic field sensors but have recently been used in vibration energy harvesting. In this paper, a new broadband vibration energy harvester has been designed and fabricated to be efficiently applicable over a range of source frequencies, which consists of two cantilever beams, two magnetoelectric (ME) transducers and a magnetic circuit. The effects of the structure parameters, such as the non-linear magnetic forces of the ME transducers and the magnetic field distribution of the magnetic circuit, are analyzed for achieving the optimal vibration energy harvesting performances. A prototype is fabricated and tested, and the experimental results on the performances show that the harvester has bandwidths of 5.6 Hz, and a maximum power of 0.25 mW under an acceleration of 0.2 g (with g = 9.8 ms^2).

Keywords : broadband vibration energy harvesting, multi-cantilever beams, magnetoelectric transducer, magnetic force

1. Introduction

Ambient energy harvesting has been in recent years the recurring object of a number of research efforts aimed at providing an autonomous solution to the powering of small scale electronic mobile devices. Among the different solutions, vibration energy harvesting has played a major role due to the almost universal presence of mechanical vibrations: from ground shaking to human movements, from ambient sound down to thermal noise induced fluctuations. The basic transduction mechanisms used for vibration-to-electricity conversion are piezoelectric [1], electromagnetic [2], electrostatic [3], or ME transductions [4, 5]. The ME transducer may be composed of magnetostrictive/piezoelectric laminate composites [6]. Magnetostrictive materials (MsM) have high energy density and high magnetomechanical coupling effect; thus, ME generators not only have the same advantage of piezoelectric generators but can also produce higher mechanical stress and power output than piezoelectric cantilever beam generators [4].

Most vibration energy harvesting devices developed to date are resonant devices whose dominant resonance frequencies are determined by the material properties and dimensions of the devices' component parts. As such, these devices tend to convert energy most effectively when the frequency of the driving vibration source closely matches the resonance frequency of the device. A frequency mismatch of only a few percent, however, results in a significant decrease in power output. In order for these energy harvesting devices to be commercially viable for many applications, they should be working over a wide frequency range. Several solutions have been proposed in the literature like active/passive frequency tuning techniques [7, 8] and widening of the bandwidth techniques [9, 10]. In active/passive tuning techniques, the easiest ways to change frequency of the device would be to alter the mass, length, or thickness of the vibrating structure. Active tuning actuators run continuously to match the harvester's resonant frequency to the source's driving frequency by providing a force that is proportional to displacement (alters the effective stiffness), or proportional to acceleration (alters the effective mass). Another solution is to widen the bandwidth of the harvester. The reported harvesters covered a wide band of external vibration frequency by implementing a number of serially connected cantilever beams with varying natural frequencies [9, 10]. Nonlinear behavior offers new capabilities to capture energy available from more complex excitations, and several recent papers demonstrated the efficacy of this approach [11, 12]. These broadening technologies in the harvesters using piezoelectric, electromagnetic and electrostatic transduction mechanisms have shown some pro-

*Corresponding author: Tel: +86 23 65111020
Fax: +86 23 65105517, e-mail: yangjin@cqu.edu.cn

mise, but they would not be applied in the harvesters using ME transducers directly due to the different transduction mechanisms.

In this paper, a new broadband vibration energy harvester using ME transducer is designed and analyzed.

2. Harvester Design and Modeling

A schematic diagram of the proposed vibration energy harvester is shown in Fig. 1. The harvester consists of two cantilever beams A and B, two ME transducers A and B, and a magnetic circuit. The magnetic circuit is made of four rectangular NdFeB magnets and two magnetic yokes, and is fixed to the housing of the harvester. The four magnets are arranged in multi-pole, head-to-tail arrangement to generate a concentrated flux gradient. The ME transducers A and B are both a sandwich of one piezoelectric layer bonded between two magnetostrictive layers, and are placed at the tip of the cantilever beams A and B, and act as the corresponding proof masses, respectively.

The two cantilever beams are initially designed to have different natural frequencies. If the source frequency matches the resonant frequency of one of the cantilever beams (with magnetic coupling), the acceleration due to the external vibration will cause relative motion between the magnetic circuit and one of the ME transducers. The ME transducer undergoes magnetic field variation in the air gap among the four magnets. In turn, the changing magnetic field causes a rotation of the quiescent magnetization vectors and the rotating magnetization vectors will generate a stress in the magnetostrictive layers. The stress is then transmitted to the piezoelectric layer, which generates electrical power. Furthermore, in this harvester, because the two ME transducers are magnetized by the magnets, there exists magnetic force between either ME

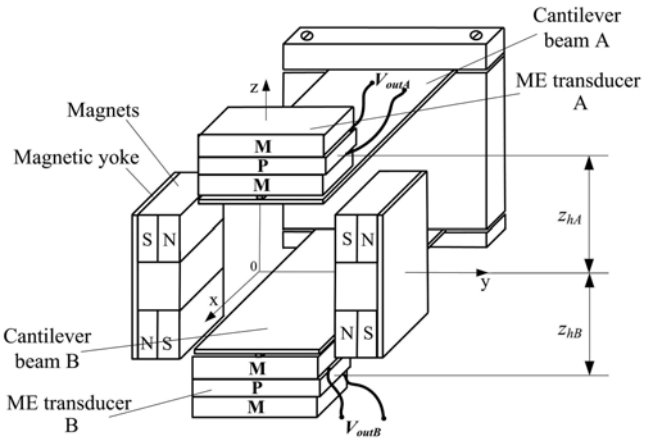

Fig. 1. Schematic diagram of the proposed vibration energy harvester.

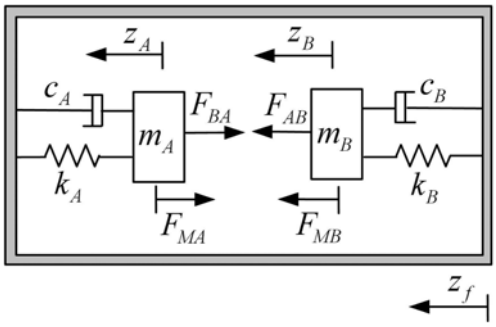

Fig. 2. Vibration model of the vibration energy harvester.

transducer and the magnetic circuit. By nonlinear behavior of the magnetic force, hardening or softening response of the cantilever beams A and B will appear in frequency response of the harvester, which allows the frequency response to be broadened in either direction [11, 12].

A two-degree-of-freedom (2DOF) mechanical spring-mass-damper model, illustrated in Fig. 2, is used to analyze the motion of the harvester. In Fig. 2, m_A and m_B are the masses at the tip of the beams A and B, respectively. The mechanical losses are modeled by the viscous damping factors c_A and c_B. k_A and k_B are the spring constants of the beams A and B, respectively. z_f is the vertical displacement of the frame, and z_A and z_B are the relative displacements of the mass A and the mass B to the frame. F_{Mk} ($k = A\sim B$) denotes the z-component of the magnetic force between the ME transducer k and the magnetic circuit. In addition, when the two ME transducers both magnetized, there exists magnetic force between each other. The corresponding magnetic forces of the ME transducers A and B are defined as F_{BA} and F_{AB}, respectively, which are the same magnitudes but in opposite directions.

The governing equations for the 2DOF harvester are given by

$$\mathbf{M}\ddot{\mathbf{Z}}+\mathbf{C}\dot{\mathbf{Z}}+\mathbf{K}\mathbf{Z}=\mathbf{F}_{z_f}+\mathbf{F}_M+\mathbf{F}_{A\_B} \tag{1}$$

where, $\mathbf{M}=\begin{bmatrix} m_A & 0 \\ 0 & m_B \end{bmatrix}$, $\mathbf{C}=\begin{bmatrix} c_A & 0 \\ 0 & c_B \end{bmatrix}$, $\mathbf{K}=\begin{bmatrix} k_A & 0 \\ 0 & k_B \end{bmatrix}$, $\mathbf{Z}=\begin{bmatrix} z_A \\ z_B \end{bmatrix}$,

$\mathbf{F}_{z_f}=\begin{bmatrix} m_A\ddot{z}_f \\ m_B\ddot{z}_f \end{bmatrix}$, $\mathbf{F}_{A\_B}=\begin{bmatrix} -F_{BA}(z_Z,z_B,z_{hA}) \\ F_{AB}(z_A,z_B,z_{hB}) \end{bmatrix}$, $\mathbf{F}_M=\begin{bmatrix} -F_{MA}(z_Z,z_B,z_{hA}) \\ F_{MB}(z_Z,z_B,z_{hB}) \end{bmatrix}$,

z_{hk} ($k = A\sim B$) denotes the initial distance between the ME transducer k and the magnetic circuit, as shown in Fig. 1. In the non-linear equations, the displacements z_A and z_B can be solved by multi-scale method [13].

The two ME transducers in the proposed harvester

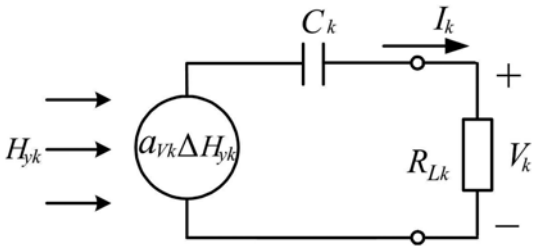

Fig. 3. Magnetoelectric equivalent circuit.

work on the L-T mode. And the magnetoelectric equivalent circuit [14] at low frequency is shown in Fig. 3. H_{yk} ($k = A\sim B$) is the external excitation magnetic field along y direction, and ΔH_{yk} is the induced magnetic field variation of the ME transducer k; I_k is the electric current; R_{Lk} is the load resistance; α_{Vk} is the ME voltage coefficient of the ME transducer k, which is defined as $\alpha_{Vk} = |dE/dH|_{H_{DC}}$ under a DC magnetic field H_{DC}; C_k is the equivalent capacitance of the ME transducer k. In Fig. 3, the voltage output and power across the load resistance R_{Lk} are

$$V_k = \left| \frac{\alpha_{Vk}\Delta H_{yk} R_{Lk}}{\frac{1}{j\omega C_k} + R_{Lk}} \right| = \frac{\alpha_{Vk}\Delta H_{yk} R_{Lk}\omega C_k}{\sqrt{1 + (\omega C_k R_{Lk})}} \tag{2}$$

$$P_k = \frac{V_k^2}{R_{Lk}} = \frac{(\alpha_{Vk}\Delta H_{yk}\omega C_k)^2 R_{Lk}}{[1 + (\omega C_k R_{Lk})^2]} \tag{3}$$

According to equation (3), the optimal load resistance can then be found by differentiating equation (3) with respect to R_{Lk}, setting the result equal to zero, and solving for R_{Lk}. Thus, the optimal load resistance is

$$R_{optk} = \frac{1}{\omega C_k} \tag{4}$$

Note that when $R_{Lk} = R_{optk}$, the harvester power output is maximum, and expressed as

$$P_{\max k} = \pi f \alpha_{Vk}^2 \Delta H_{yk}^2 C_k \tag{5}$$

According to equations (2) and (5), in order to achieve a large voltage output and power, the magnet circuit in Fig. 1 should provide the ME transducers to work in the optimum DC magnetic bias field to obtain the optimal ME voltage coefficient α_{Vk}, and the ME transducers should undergo large enough magnetic field variation ΔH_{yk} at a small relative displacement.

3. Simulation and Analysis

In order to obtain the optimal energy harvesting performances, the effects of the non-linear magnetic forces and the distribution of the magnetic field on the voltage output and the frequency response of the harvester are investigated. The soft of Ansoft's Maxwell 3D is employed to simulate and analyze the magnetic forces and the magnetic field. The simulation model is shown in Fig. 1. The dimension of each magnet is 6 mm × 6 mm × 2.5 mm. The distance between the upper magnet and the lower magnet is 2.5 mm, and that between the left magnet pole and the right one is 14mm. Each ME transducer is the sandwich of one $Pb(Mg_{1/3}Nb_{2/3})O_3-PbTiO_3$(PMNT) layer (12 mm × 6 mm × 0.8 mm) bonded between two Terfenol-D layers (12 mm × 6 mm × 1 mm). The piezoelectric layer is polarized in its thickness direction, and the Terfenol-D layers are magnetized along the longitudinal direction.

3.1. Frequency analysis

Because the two ME transducers are both fixed to the cantilever beams, the magnetic forces of the ME transducers will result in corresponding additional stiffness on the beams. The magnitudes of the corresponding magnetic stiffness, k_{magA} and k_{magB}, can be written in terms of the changes in magnetic forces as a function of distances as [8]

$$k_{magA} = \left| \frac{d(F_A(z_{hA}))}{dz_{hA}} \right| \tag{6a}$$

$$k_{magB} = \left| \frac{d(F_B(z_{hB}))}{dz_{hB}} \right| \tag{6b}$$

where $F_A = F_{MA} + F_{BA}$ and $F_B = F_{MB} + F_{AB}$.

Therefore, the effective stiffness vector $\mathbf{K}_{eff}$ with respect to the beams A and B is

$$\mathbf{K}_{eff} = \begin{bmatrix} k_A + \operatorname{sgn} x \cdot k_{magA} & 0 \\ 0 & k_B + \operatorname{sgn} x \cdot k_{magB} \end{bmatrix} \tag{7}$$

where the sign of the sgn$x$ is dependent on the mode of the magnetic force (i.e. positive for the repulsive magnetic mode and negative for the case of the attractive magnetic mode) [8]. For the case of the magnetically-altered stiffness, the resonant frequencies of the beams A and B become

$$\begin{bmatrix} \omega_{A\_eff} \\ \omega_{B\_eff} \end{bmatrix} = \begin{bmatrix} \sqrt{\frac{k_A + \operatorname{sgn} x \cdot k_{magA}}{m_A}} \\ \sqrt{\frac{k_B + \operatorname{sgn} x \cdot k_{magB}}{m_B}} \end{bmatrix} \tag{8}$$

Fig. 4 shows the simulation results of the magnetic force F_A of the ME transducer A for different z_{hA} and z_{hB}

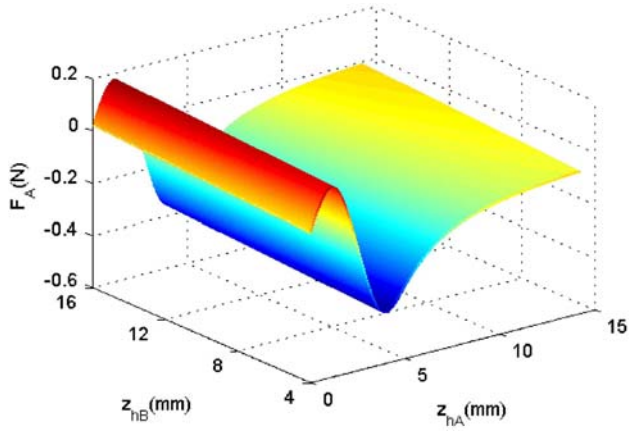

Fig. 4. Magnetic force F_A of the ME transducer A.

values. It can be seen that, the variations of the magnetic force F_A with z_{hA} have the same regularity for different initial distances z_{hB}. Therefore, in Fig. 5 we plot the magnetic force F_A and the additional magnetic stiffness k_{magA} versus z_{hA} for a fixed value of z_{hB}. In this figure, it is clear that, 1) when z_{hA} is changed from 0 to 2.2 mm, the mode of the magnetic force F_A is always repulsive, and the sign of the sgn$x$ of the additional stiffness k_{magA} in equation (7) is positive. The effective resonant frequency of the beam A in equation (8) will be tuned to be higher than that of the beam with no magnetic coupling. 2) When z_{hA} is beyond 2.2 mm, the mode of the magnetic force F_A is changed to be attractive. k_{magA} will alter the effective resonant frequency to be lower than that of the beam A (no magnetic coupling) except when z_{hA} is 4.2 mm. At $z_{hA} = 4.2$ mm, the magnitude of the magnetic force F_A reaches maximum, but the corresponding additional stiffness k_{magA} is zero. As a consequence, the resonant frequency of the beam A will remain unchanged. Furthermore, it is obvious that the effect of F_B on the

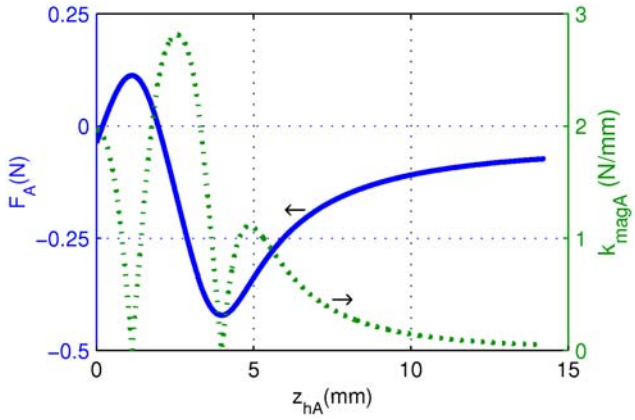

Fig. 5. Magnetic force F_A and additional stiffness k_{magA} versus z_{hA} for a fixed value z_{hB}.

frequency of the beam B is the same to that of F_A on the beam A.

3.2. Distribution of magnetic field

According to eqs. (2) and (5), in order to obtain a large ME conversion output, the magnet circuit should provide the transducers to work in the optimum condition of the DC magnetic bias fields, and the ME transducers should undergo large enough magnetic field variations at small relative displacements. Therefore, the distribution of the magnetic field in the air gap is analyzed in this section by Ansoft's Maxwell. In simulation, the parameters of the harvester are the same as that in section 3.1.

Fig. 6 plots the magnetic flux lines of the ME transducers and the magnets when z_{hA} and z_{hB} are 5.2 mm. Fig. 7 shows the induced magnetic flux density $\overline{B}_A(z_{hA})$ of the ME transducer A for different z_{hA} and z_{hB} values. It can be seen that, the variations of $\overline{B}_A(z_{hA})$ with z_{hA} have the same regularity for different initial distances z_{hB}. Therefore, in Fig. 8 we plot $\overline{B}_A(z_{hA})$ and the variation of $\overline{B}_A(z_{hA})$ for a fixed value of z_{hB}. As can be seen from Fig.

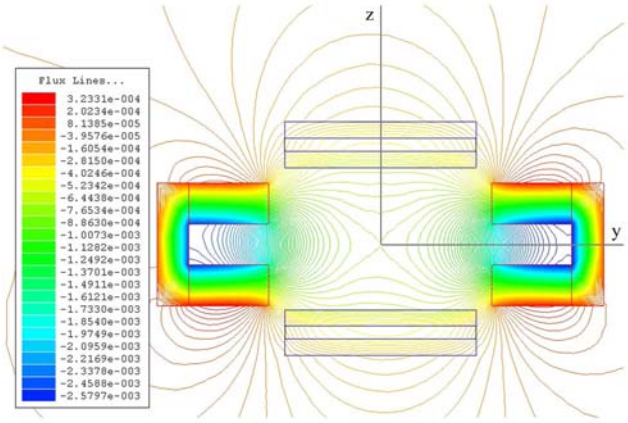

Fig. 6. Magnetic flux lines of the ME transducers and the magnets.

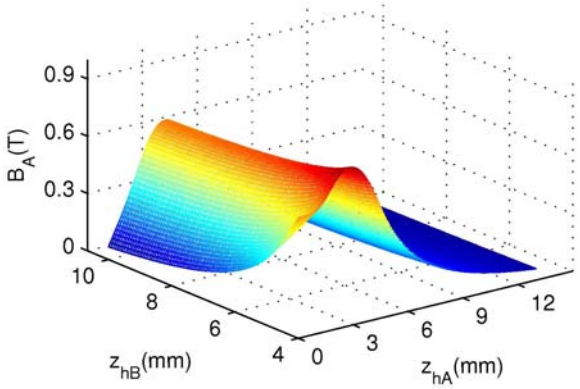

Fig. 7. Magnetic flux density of $\overline{B}_A(z_{hA})$.

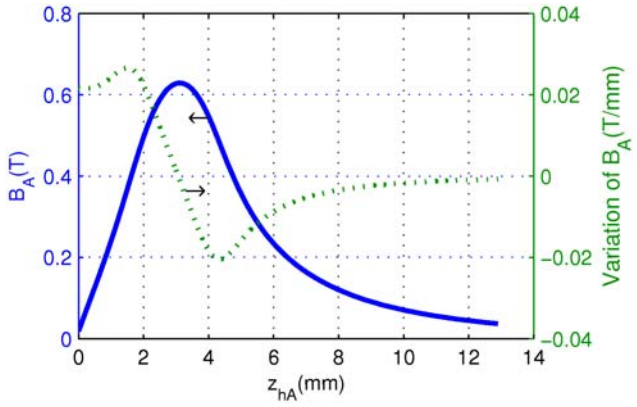

Fig. 8. Variation of $\overline{B}_A(z_{hA})$: (a) Harvester prototype; (b) Block diagram of the setup.

8, the variation of $\overline{B}_A(z_{hA})$ presents two peaks at z_{hA} = 1.7 mm and 4.2 mm, and the absolute peak values reach around 0.026T/mm and 0.020T/mm, respectively. These two distances (z_{hA} = 1.7 mm and 4.2 mm) may be used as the optimal initial positions to place the ME transducer A to generate high voltage output, if the ME transducer can work in the best condition of the DC bias field at these positions. In addition, the effect of the distance z_{hB} on the magnetic flux density $\overline{B}_B(z_{hB})$ of the ME transducer B is the same to that of z_{hA} on the ME transducer A.

4. Experiment and Result

The cantilever beams A and B are both made up of 10 mm × 10 mm × 0.5 mm beryllium bronze. The dimensions of NdFeB magnets are 6 mm × 6 mm × 2.5 mm. The remnant flux density (Br) and the relative permeability of the magnet are 1.2 T and 1.05, respectively. Each ME transducer is the sandwich of one PMNT layer (12 mm × 6 mm × 0.8 mm) bonded between two Terfenol-D layers (12 mm × 6 mm × 1 mm). The ME transducers are bonded using an insulated epoxy adhesive, and cured at 80°C for 1 h under load to provide a strong bond between the layers. Fig. 9 shows the experimental set-up. A vibration shaker is used to supply mechanical vibrations to the prototype. An accelerometer is mounted in the vibration shaker to measure the acceleration of vibrations applied to the prototype. The voltage output of the prototype is measured and stored by a Tektronix TDS2022B digital storage oscilloscope. In all measurements, the shaker table acceleration is set to 0.2 g.

In experiment, the ME transducer A is placed at the end of the cantilever beam A with the natural frequency of 29.2 Hz. The natural frequency of the cantilever beam B with the ME transducer B is 32.6 Hz. In addition, the beams A and B are fixed on clamps that can be vertically displaced using screw-spring mechanism to change the initial distances z_{hA} and z_{hB}. Fig. 10 plots the measured peak-to-peak voltages of the ME transducers A and B for three different values of z_{hA} when z_{hB} is a fixed value of 4.2 mm.

In Fig. 10, it can be seen that: 1) Because the frequency response of the beam B is mainly dependent on the initial distance z_{hB}, when z_{hB} is a fixed value, the frequency responses of the beam B are almost unchanged when z_{hA} is altered from 2.0 mm to 5.2 mm. In addition, when z_{hB} = 4.2 mm, k_{magB} is zero, and the resonant frequency of the beam B is equal to the corresponding natural frequency of 32.6 Hz, as analyzed in section 3. 2) In Fig.10(a), when z_{hA} = 2.0 mm, it is observed that the resonant frequency (49.0 Hz) of the beam A is higher than the natural frequency (29.2 Hz) as the repulsive mode of the magnetic force F_A is applied. 3) In Fig. 10(b), when z_{hA} = 5.2 mm, due to the attractive mode of the magnetic force F_A, the resonant frequency (27.2 Hz) of the beam is lower than the natural frequency (29.2 Hz). 4) In Fig. 10(c),

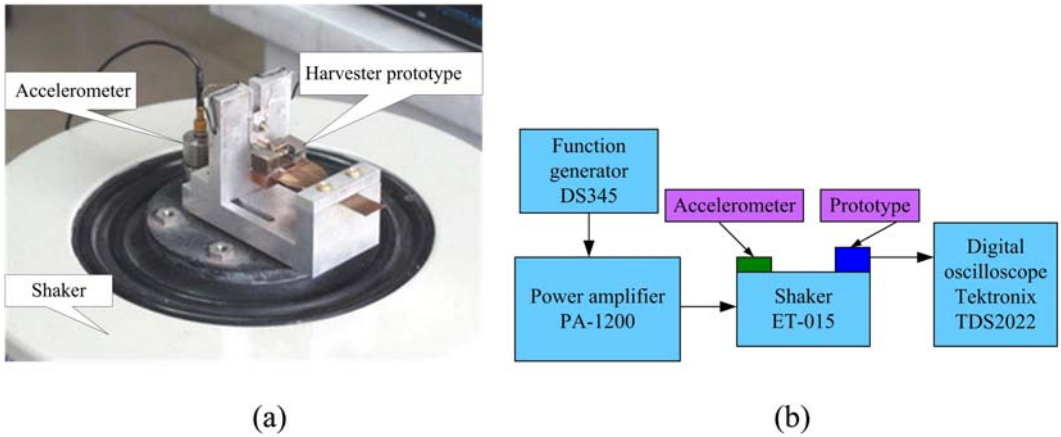

Fig. 9. Experimental setup.

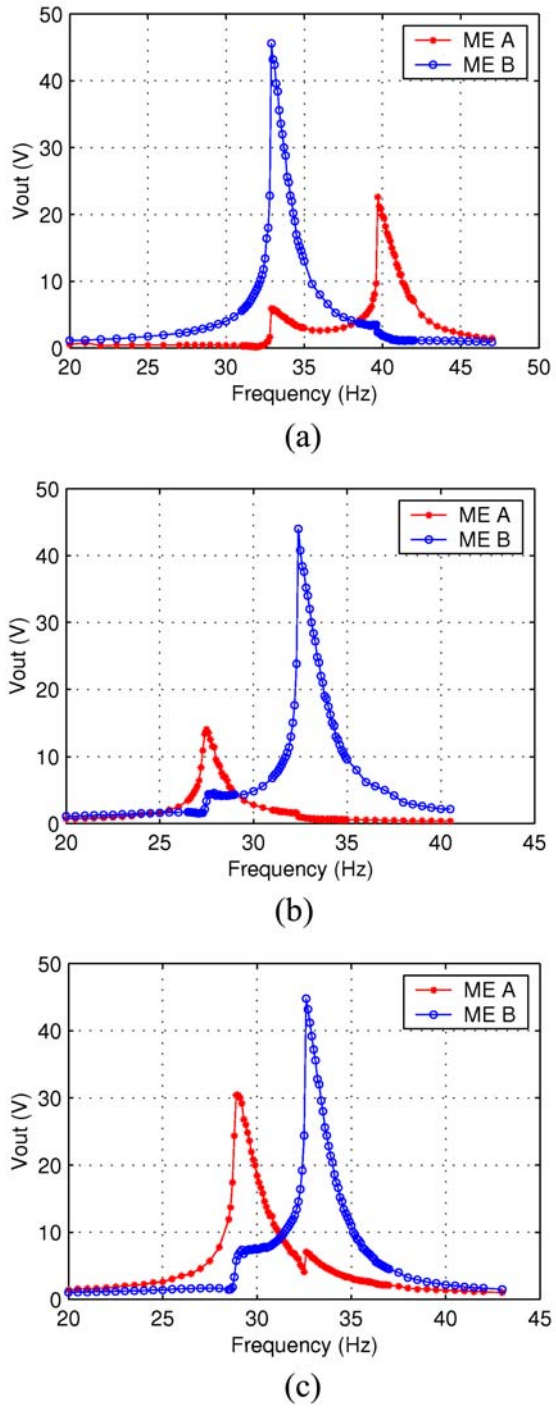

Fig. 10. Voltage outputs versus frequency for different values of z_{hA}: (a) $z_{hA} = 2.0$ mm, $z_{hB} = 4.2$ mm; (b) $z_{hA} = 5.2$ mm, $z_{hB} = 4.2$ mm; (c) $z_{hA} = 4.2$ mm, $z_{hB} = 4.2$ mm.

when $z_h = 4.2$ mm, because the additional stiffness k_{magA} is zero, the resonant frequency of the beam A is unchanged and equal to the corresponding natural frequency. Further, the two resonance peaks of the beams A and B overlap to successfully widen the bandwidth of the harvester. And by nonlinear behaviors of the magnetic forces F_A and F_B, the softening responses of the beams A and B appear in Fig. 10(c), which allow the frequency responses to be also broadened [11, 12]. In this case, the harvester shows a 3dB bandwidth of 5.6 Hz. 5) In Fig. 10, when one cantilever beam is in resonant condition and the corresponding ME transducer has maximum voltage output, another ME transducer will also generate voltage output. This is because that the ME transducer at the resonant cantilever beam will provide changing magnetic field for another ME transducer, which undergoes the changing magnetic field to generate voltage output. This phenomenon improves the total voltage output of the harvester.

Using the measured voltage outputs, the power of the harvester is estimated by the model in [8]. The maximum power of 0.25 mW is achieved when $z_{hA} = z_{hB} = 4.2$ mm. As mentioned in section 3, when the initial positions z_{hA} and z_{hB} both are 4.2 mm, the two ME transducers can undergo the largest magnetic field variations to generate the highest power outputs.

5. Conclusion

This study presents a new broadband vibration energy harvester using ME transducers, which takes advantage of multi-cantilever beams and the nonlinear behavior of the magnetic force to expand the working bandwidth in ambient low frequency vibration. The harvester showed a bandwidth of 5.6 Hz and a maximum power of 0.25 mW under acceleration of 0.2 g. The principle may be generally applied to improve the frequency bandwidth of the energy harvesting system that works using ME transductions.

Acknowledgments

This work was supported by the National Natural Science Foundation of China (No. 50830202, 60774055, 10776039).

References

[1] P. Glynne-Jones, S. P. Beeby, and N. M. White, IEE Proc. Measure. Technol. **148**, 68 (2001).
[2] R. Torah, P. Glynne-Jones, M. Tudor, T. O'Donnell, S. Roy, and S. Beeby, Meas. Sci. Technol. **19**, 125202 (2008).
[3] N. H. Ching, H. Y. Wong, J. Li, H. W. Leong, and Z. Wen, Sens. Actuators: A **97-98**, 685 (2002).
[4] J. Huang, R. C. O'Handley, and D. Bono, Proc. SPIE **5050**, 229 (2003).
[5] X. Z. Dai, Y. M. Wen, P. Li, J. Yang, and G. Y. Zhang,

Sens. Actuators: A **156**, 350 (2009).
[6] T. Li, S. W. Or, and H. L. Chan, J. Magn. Magn. Mater. **304**, e442 (2006).
[7] E. S. Leland and P. K. Wright, Smart Mater. Struct. **15**, 1413 (2006).
[8] V. R. Challa, M. G. Prasad, Y. Shi, and F. T. Fisher, Smart Mater. Struct. **17**, 015035 (2008).
[9] I. Sari, T. Balkan, and H. Kulah, Sens. Actuators: A **145-146**, 405 (2008).
[10] J. Q. Liu, H. B. Fang, Z. Y. Xu, X. H. Mao, X. C. Shen, D. Chen, H. Liao, and B. C. Cai. Microelectron. J. **39**, 802 (2008).
[11] S. C. Stanton, C. C. McGehee, and B. P. Mann, Appl. Phys. Lett. **95**, 174103 (2009).
[12] X. Xing, J. Lou, G. M. Yang, O. Obi, C. Driscoll, and N. X. Sun, Appl. Phys. Lett. **95**, 134103 (2009).
[13] M. Vidyasagar, Nonlinear systems analysis, Prentice Hall, Englewood Cliffs, New Jersey (1993) pp. 33~127.
[14] L. X. Bian, Y. M. Wen, P. Li, Q. L. Gao, and X. X. Liu, J. Magnetics **14**, 66 (2009).